Materials & Design 242 (2024) 112979

Contents lists available at ScienceDirect

Materials & Design

journal homepage: www.elsevier.com/locate/matdes

Design–material transition threshold of ribbon kirigami

Yao Chen [a,b,*], Ruoqi He [b], Shun Hu [b], Ziyang Zeng [c], Tong Guo [b], Jian Feng [a], Pooya Sareh [d,e,f,*]

[a] Key Laboratory of Concrete and Prestressed Concrete Structures of Ministry of Education, and National Prestress Engineering Research Center, Southeast University, Nanjing 211189, China
[b] School of Civil Engineering, Southeast University, Nanjing 211189, China
[c] Department of Mathematics, National University of Singapore, Singapore 119076, Singapore
[d] Creative Design Engineering Lab (Cdel), School of Engineering, Newcastle University, Newcastle upon Tyne NE1 7RU, United Kingdom
[e] School of Engineering, University of Liverpool, Liverpool L69 3GH, United Kingdom
[f] Escuela Técnica Superior de Ingeniería y Diseño Industrial, Universidad Politécnica de Madrid (UPM), Madrid 28012, Spain

ARTICLE INFO

Keywords:
Ribbon kirigami
Shape-shifting metastructure
Ductility of metamaterials
Geometric design optimization
Design–material transition (DMT) threshold

ABSTRACT

The ribbon kirigami pattern has garnered significant attention over the past decade because of its interesting geometric and mechanical properties such as extreme elongation and high ductility, making it a viable choice for various applications such as developing medical devices and flexible electronics. Despite the promising prospects of this type of morphing structure, its deformation mechanism and sensitivity to materials properties and geometric parameters have remained largely unexplored. Here we take a computational approach to studying the deformation process and ductility of a typical ribbon kirigami metastructure. To this end, the deformation process is divided into various stages. We demonstrate the existence of a certain threshold of the process at which the deformation behavior starts to be dominated by the properties of the constituent material, after the initial geometric-design-dominated stages. This turning point, called the design–material transition (DMT) threshold, determines a key limit in the deformation capacity of such metastructures for practical applications. Based on the introduced deformation mechanism, an elongation prediction model is derived for the metastructure, followed by conducting experiments to validate the accuracy of the model. Furthermore, a genetic algorithm and an interior-point method are utilized to develop an efficient algorithm for the optimization of the geometric parameters of the kirigami pattern. We anticipate that the findings of this study open a path to engineering functional kirigami patterns for the design and fabrication of highly ductile shape-shifting structures.

1. Introduction

Over the past few decades, shape-shifting structures have significantly attracted the attention of research communities across various branches of science and engineering [1–14]. Particularly, the ancient arts of origami and kirigami have been applied to designing a wide range of shape-shifting structures and systems [15–28]. Origami is generally used as a technique to transform flat sheets of material into complex three-dimensional structures by folding along carefully designed crease lines [29–33]; this results in the development of structures with tailored geometric and mechanical properties, exemplifying a remarkable synergy between form and function in engineering design [34–38]. There is a wide range of approaches to designing origami crease patterns, including numerical methods based on computational geometry [39–46], group-theoretic techniques [47–51], and optimization-based approaches [52,53].

Kirigami is a variation of origami in which the designer is allowed to cut the paper in addition to folding it. It is conventional to create two- or three-dimensional kirigami-inspired structures by cutting slits [6,54,55] on flat sheets of materials, while the formed strips allow for further deformation of the structure. It has been found that, in many cases, it is unnecessary to maintain the integrity of the material face, which enables designers to develop structures with a range of interesting properties such as negative Poisson's ratio [56–59], ultra-high ductility [60,61], and programmability [62–64]. Notably, such a relatively simple fabrication method of cutting slits into planar sheets of material has recently led to the creation of complex, programmable patterns on the nanometer scale [65,66].

* Corresponding authors at: School of Civil Engineering, Southeast University, Nanjing 211189, China (Y. Chen); Creative Design Engineering Lab (Cdel), School of Engineering, Newcastle University, Newcastle upon Tyne NE1 7RU, United Kingdom (P. Sareh).
E-mail addresses: chenyao@seu.edu.cn (Y. Chen), pooya.sareh@ncl.ac.uk (P. Sareh).

https://doi.org/10.1016/j.matdes.2024.112979
Received 29 February 2024; Received in revised form 15 April 2024; Accepted 23 April 2024
Available online 26 April 2024

In general, kirigami structures can be classified into five types [65]: fractal-cut kirigami [64,67–69], ribbon kirigami [3,70], lattice kirigami [71,72], zigzag kirigami [73], and closed-loop kirigami [74] (Fig. 1a). Among them, in the last decade, ribbon kirigami structures have received particular attention because of their interesting geometric characteristics and ultra-high ductility (Fig. 1b). More specifically, to improve structural ductility, ribbon kirigami patterns have been introduced into the design of different material systems such as graphene [75,76], metallic glasses [77–79], nanocomposites [80], thermoset shape-memory polyurethane [81], and MoS_2 [82]. At an applied level, ribbon kirigami structures have been used in stretchable batteries [83–86], soft machines [87,88], optical tracking systems [89,90], building skins [64,91], and wearable and implantable devices [92,93]. Inspired by the studies of Lamoureux et al. [89] and Tang et al. [64], Fig. 1c illustrates a smart curtain system exploiting the ductility of a ribbon kirigami structure equipped with flexible photovoltaic panels. When sunlight shines on the curtain, the photovoltaic panels convert it into electrical energy. The generated electricity can power the actuating device, thereby controlling the curtain to align the panels vertically with the sunlight and achieve maximum power generation efficiency. In addition, the curtain system can meet different lighting requirements by adjusting the amount of sunlight.

Having such a wide range of potential applications, understanding and exploiting the mechanical properties of ribbon kirigami structures have been of particular interest over the past few years. Han et al. [94] proposed a critical force prediction model based on the beam deflection theory and introduced a force concentration parameter to predict the nominal ultimate force of kirigami metallic glasses. Moshe et al. [95] presented a geometric approach to the mechanics of perforated thin elastic sheets and introduced a kirigami design principle to selectively relax stresses in elastic materials. Chen et al. [96] proposed a finite element analysis (FEA) approach to obtaining the apparent elastic limit of kirigami metallic glasses, providing a flexible method to analyze their mechanical properties. Isobe and Okumura [97] used the Landau theory of continuous thermodynamic transitions to analyze the behavior of kirigami structures, demonstrating that their mechanical response can be explained using the tools of statistical physics.

In this paper, we report the findings of a study on the ductility of a ribbon kirigami structure and the relationship between its geometric parameters and elongation behavior. We model the deformation mechanism of the kirigami structure as a multi-stage process. Moreover, the ending point of the fourth stage, defined as the *design–material transition* (*DMT*) *threshold*, is shown to be the limitation of deformation in practice. Besides, an elongation prediction model is derived based on the deformation mechanism. To verify the FEA results and prediction model, physical experiments are designed and conducted. In addition, a genetic algorithm (GA) and the interior-point method (IP) are used to develop a geometric design optimization algorithm considering

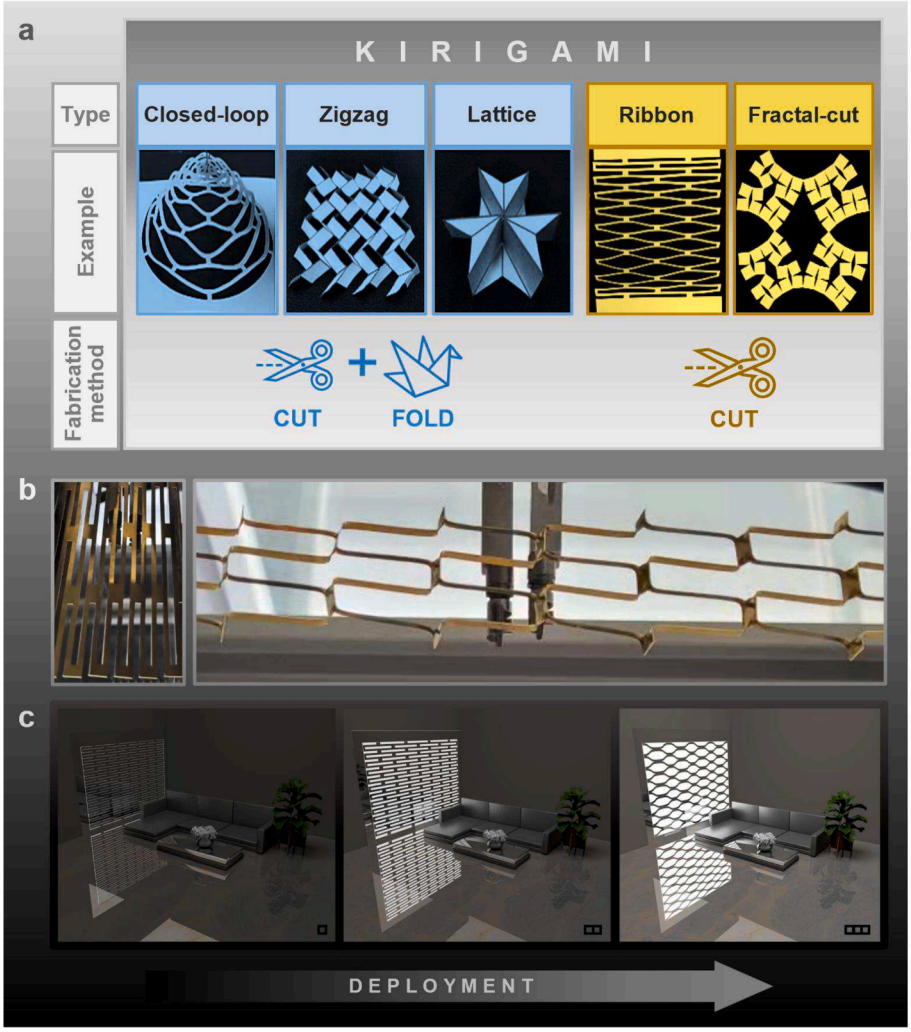

Fig. 1. An overview of a range of conventional kirigami structures. (**a**) Classification of kirigami structures based on their fabrication methods (adapted from [65]). (**b**) A typical ribbon kirigami structure made of brass in two different deformation states. (**c**) Computer-aided artist's impression of a smart curtain system capable of meeting different lighting and heating requirements by adjusting the amount of sunlight.

different design requirements.

2. Results and discussion

2.1. Deformation process

A parallel-cut kirigami pattern composed of n units is presented in Fig. 2a, where three parameters a, b, and c determine the geometry of the unit. Dias et al. [98] showed that thickness has a negligible effect on the deformation response of ribbon kirigami mertastructures; thus, thickness is not included as a geometric parameter in this study. Here we consider a base model with a=32.5 mm, b=10 mm, c=2.5 mm, and n=8. This model is constructed from Q235 steel, the material properties of which are provided in Section 2.4. Using finite element analysis (FEA), the deformation process can be delineated into six different stages (Fig. 2b), described below as stages S_1 to S_6. Furthermore, Fig. 2c shows the stress response of the structure at stages S_2, S_3, S_4, and S_5, obtained from the FEA simulations.

S_1: *Strain-energy accumulation stage*. The ribbon kirigami structure experienced in-plane deformation with displacement loading, while stress concentration occurred at the hub-strip connections. The external force did work on the structure, transforming into strain energy accumulated at the connections. At this stage, strains were mainly elastic, and the model could return to its original state after the external force was removed.

S_2: *Strain-energy release stage*. The strain energy was released as

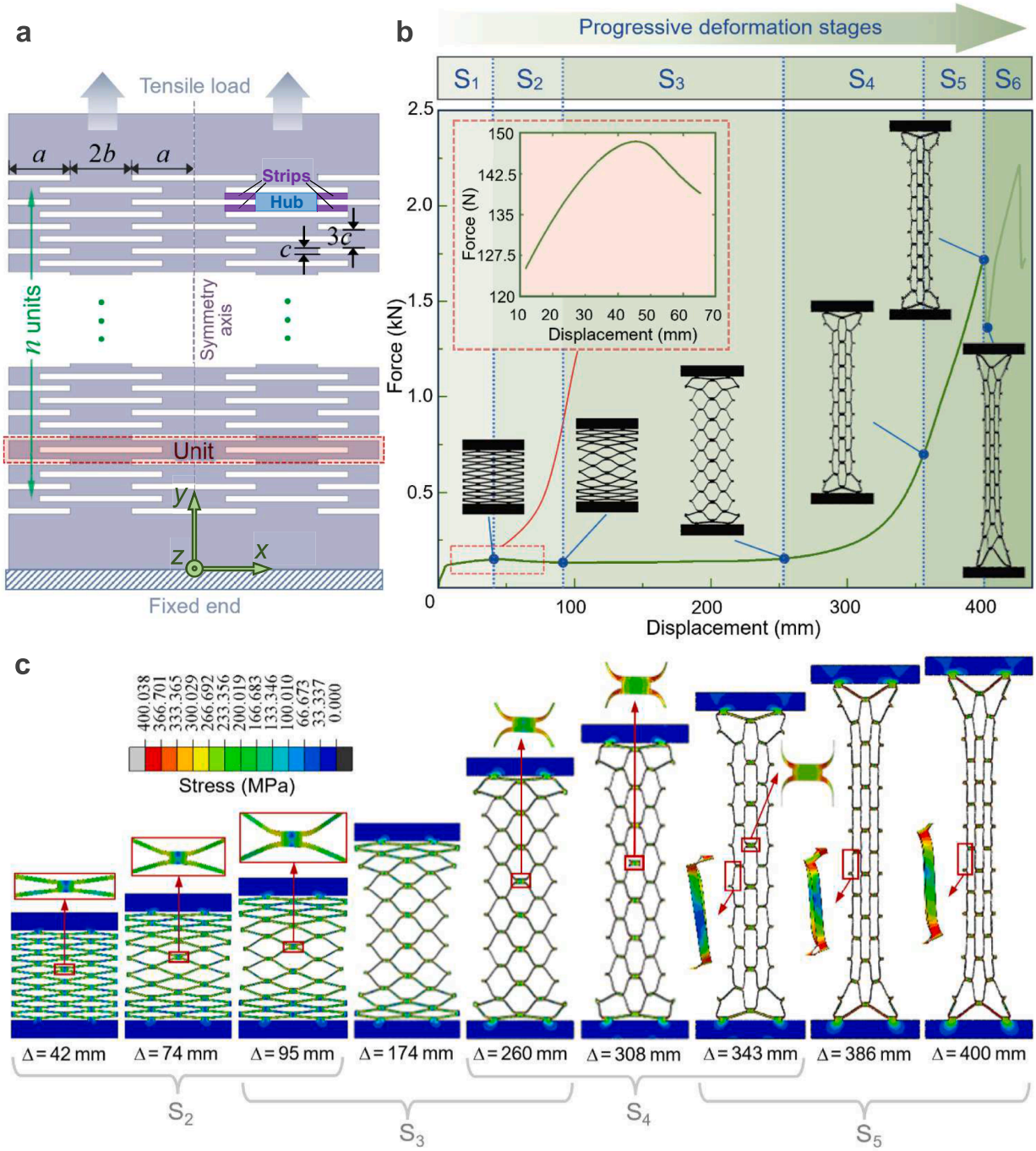

Fig. 2. Modeling and behavior analysis of a typical ribbon kirigami metastructure. (**a**) Geometric model. (**b**) Deformation process of the ribbon kirigami structure made of Q235 steel simulated using FEA. (**c**) Stress response of the ribbon kirigami structure at stages S_2, S_3, S_4, and S_5, obtained from the FEA simulations.

displacement increased. When the hub-strip connections reached the yield stress, they entered the yielding stage, and the subsequent plastic deformations in the yielding areas enhanced the rotational capacity of the strips. Besides, the release of strain energy diminished the stresses around the hubs, thereby leading to the reduction of the resultant force.

S_3: *Deformation development stage*. The structure showed ultra-high ductility and quasi-zero stiffness at this state. As can be seen from Fig. 2c, the strips rotated with increasing displacement, whereas the hubs started to warp out of the tensile plane. As displacement increased, the angles between the strips and the *xy*-plane gradually increased. At this stage, the rotation of the strips dominated the deformation, resulting in a constant resultant force with displacement loading, as shown in Fig. 2b.

S_4: *Rotation stage*. With the displacement increasing, the rotational capacity of the plastic hinges could not meet the rotation of the strips. As a result, the plastic zone expanded at the hubs to improve the rotational capacity of the structural elements. In the initial stages of loading, the strip was aligned parallel to the *x*-axis. As displacement was applied, the strips rotated around the hub joints, eventually becoming parallel to the *y*-axis (i.e., the projected angles between the strips and the hubs in the *yz*-plane reached 90°). It was worth noting that the first four stages dominated the deformation process of the ribbon kirigami structure, as can be seen in Fig. 2b.

S_5: *Material performance stage*. After the first four stages of rotation, the strips turned vertical; thus, the deformation capacity derived from the geometric design reached maximum. At this stage, the properties of the constituting material began to dominate the deformation behavior of the structure. As the displacement increased, the angles between the strips and the *xy*-plane decreased, while the angles between the strips and the hubs increased. In addition, the elastic stress in the strips increased, leading to an almost linear force–displacement curve. Furthermore, the plastic areas entered the strengthening phase, with the hubs fracturing as the stress reached the ultimate tensile strength. At this stage, the elastic strain of the strips dominated the deformation of the structure, resulting in a constant overall stiffness.

S_6: *Fracture development stage*. Following the emergence of the fracture location, the structure underwent stress redistribution, while the resultant force decreased sharply. With the displacement increasing, the structure tended to form another fracture location, and subsequently, it exhibited the same properties as the fifth stage.

2.2. Design-material transition (DMT) threshold

From the previous section, we can observe that the deformation in the first four stages is mainly due to the elongation caused by the rotation of the strips. At the end of the fourth stage, the rotation of the strips ceases, and they become parallel to the *y*-axis. Therefore, the maximum elongation in the first four stages predominantly depends on the length of strips and hubs. Hence, it can be concluded that the deformation capacity of the structure in the first four stages of deformation is primarily determined by the initial geometric design parameters. As illustrated in Fig. 3, the results of FEA also show that the displacement ranges corresponding to the third and fourth stages are qualitatively similar. However, the figure also reveals that the deformation responses of different structures exhibit significant differences in the fifth stage, implying that they are heavily reliant on the properties of the constituent materials after the fourth stage. According to FEA results, the plastic deformation region is tiny and primarily concentrated at the hubs. This observation is in agreement with the findings of a recent study [79] showing that the strain energy loss of the ribbon kirigami structure is insignificant.

After removing the external force, the residual deformation is minimal and concentrated at the hubs. However, the strain energy loss and plastic deformation both substantially increase when the displacement reaches the fifth stage, leading to a drastic reduction in the deformation capacity. Thus, the ending point of the fourth stage is crucial for analyzing the deformation mechanism of ribbon kirigami metastructures, and we define it as the *design-material transition (DMT) threshold*.

During the deformation process, plasticity mainly impacts the peak stress of stage S_2 and the ductility of stage S_5. The greater the yield strength (i.e., the stress at which plastic deformation begins) of the material, the higher the peak stress of stage S_2. This can be corroborated by the force–displacement curves of five different elastoplastic materials in Fig. 3, where stainless steel has the highest yield strength and correspondingly the highest peak stress in stage S_2. On the other hand, aluminium alloy 3003 (Al-3003), mild steel, and Q235 steel have close yield stresses, leading to nearly identical peak stresses in stage S_2.

Furthermore, the ultimate strain of the material (i.e., the strain corresponding to fracture) influences the development of stage S_5. Importantly, the plastic deformation significantly increases in stage S_5, which makes the structural deformability predominantly dependent on the plastic deformation capacity of the material. Taking stainless steel as an example, its limited ultimate strain (0.002) makes its structural plastic deformability extremely limited, resulting in poor ductility in stage S_5. Therefore, the structure exhibits fracture after stage S_4, manifesting as a substantial drop in force.

To further validate the aforementioned analysis, we referred to the

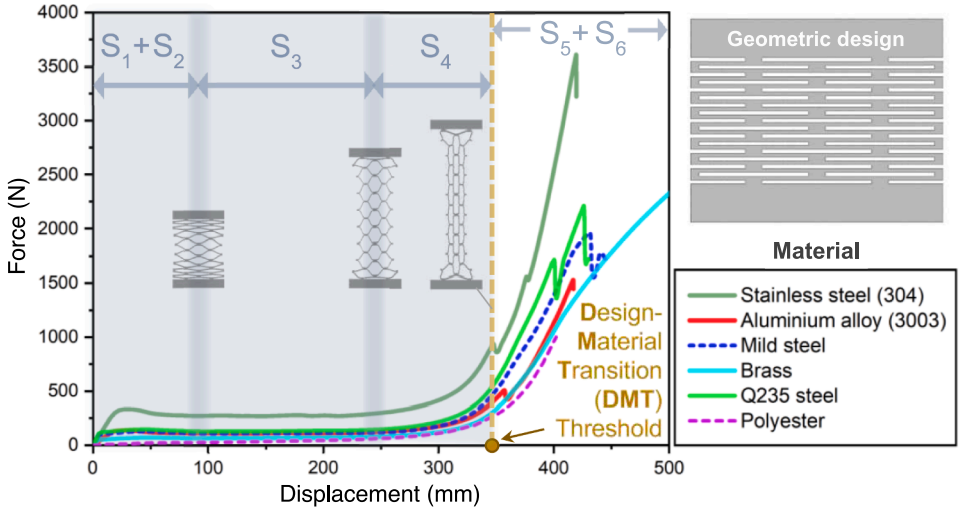

Fig. 3. Force-displacement curves of six geometrically identical ribbon kirigami metastructures made of different materials.

previous studies presented in [67,99] and conducted a simulation using polyester with an elastic material model. It is worth noting that in the elastic model, there are no plastic hinges formed during deformation, hence there is no differentiation between the first two stages. In other words, given that the boundary between stages S_1 and S_2 is determined by the local peak stress point, and as the elastic model does not include any yielding point, there will be no distinct boundary between the first two stages; therefore, they can be considered as a single stage S_1+S_2, as illustrated in Fig. 3. Notably, the DMT threshold in the elastic material model aligns well with that of the elastoplastic materials, confirming that the threshold mainly depends on the geometric design of the structure.

2.3. Elongation prediction model

From the discussion above, it can be concluded that the deformation capacity of ribbon kirigami metastructures is dominated by geometric parameters at the first four stages, whereas the choice of material has a relatively marginal impact. In particular, the DMT threshold is a critical turning point in the deformation process.

Here, we aim to develop a prediction model for the elongation of a typical ribbon kirigami structure. To this end, a typical ribbon kirigami structure in its initial configuration is illustrated in Fig. 4a. The Geometric parameters of this configuration are designated in Fig. 4b. Assuming a tensile loading is applied, the schematic of the structure in an elongated configuration is depicted in Fig. 4c along with its corresponding geometric parameters.

Despite the relatively simple geometry, the structure exhibits strong nonlinear deformation characteristics, posing significant challenges to its deformation prediction. To tackle these challenges, based on numerical and experimental observations, we consider two assumptions that introduce slight errors but can considerably alleviate the difficulty of developing the prediction model. First, we neglect the curvature of the strips at the hub-strip connections, assuming the entire body of each strip is parallel to the *yz*-plane. Second, the change in the length of the two end parts after deformation, l_e, is neglected. Importantly, the first assumption, which overlooks the influence of curvature, tends to overestimate the predicted values when compared to the actual values. Conversely, the second assumption, by disregarding the elongation of the end parts, results in an underestimation. As a result, the errors from these two simplifications can partially counterbalance each other. More importantly, the length discrepancies caused by these errors are substantially smaller than the total length change of the structure. Additionally, Section 2.5 validates the accuracy of the prediction model through an experimental approach; therefore, these two approximations have a minimal impact on the precision of the predictive model.

At the DMT threshold, the angle between the hubs and the *xy*-plane reaches its maximum value, defined as the *critical angle* θ_c, as shown in

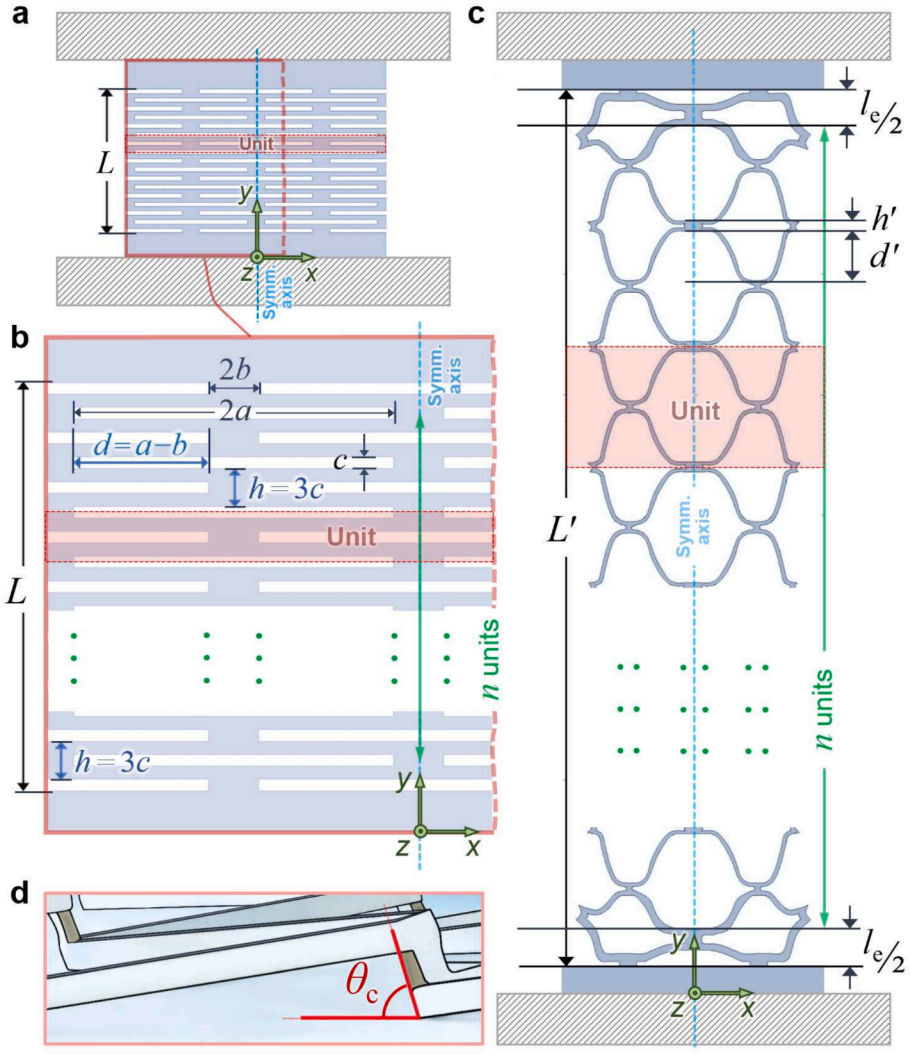

Fig. 4. Geometric analysis of a typical ribbon kirigami metastructure. (**a**) Initial configuration. (**b**) Geometric parameters of the initial configuration. (**c**) Geometric parameters of the structure in an elongated configuration. (**d**) The critical angle at the DMT threshold.

Fig. 4b. Furthermore, the strips are at 90° to the hubs. In addition, the projections of the strips on the *xy*-plane are parallel to the *y*-axis. The critical angle can be obtained from the geometric conditions as follows

$$\theta_c = \tan^{-1}\left(\frac{a-b}{3c}\right) \tag{1}$$

$$X = \frac{a-b}{3c} \tag{2}$$

where the *geometric ratio X* is a dimensionless coefficient related to geometric parameters.

The original length of the structure is L, while its length after deformation is L', including the length of the end parts l_e, the projection length of the hubs H', and the projection length of the strips D'. Since the deformation of the end units is neglected, l_e remains invariant. Based on Fig. 4, we can write

$$L = (4n+1)c \tag{3}$$

$$L' = D' + H' + l_e \tag{4}$$

The original length of a single hub h is 3c. Considering the warping of the hubs, the length of the projection of a single hub on the *xy*-plane, h', is

$$h' = 3c\cos\theta_c \tag{5}$$

The number of hubs is $2n-3$, excluding the end hubs. Therefore, the total length of the hubs after deformation is

$$H' = \sum_{i=1}^{2n-3} h_i' = 3c(2n-3)\cos\theta_c \tag{6}$$

The original length of a single strip d is $a-b$. Considering the warping of the strips, the projection length of a single strip on the *xy*-plane, d', is

$$d' = (a-b)\sin\theta_c \tag{7}$$

The number of strips is $2n-2$, excluding the end strips. Therefore, the total length of the strips after deformation is

$$D' = \sum_{i=1}^{2n-2} d_i' = 2(n-1)(a-b)\sin\theta_c \tag{8}$$

The length of the elongated ribbon kirigami is

$$L' = H' + D' + l_e = 3c(2n-3)\cos\theta_c + 2(n-1)(a-b)\sin\theta_c + 8c \tag{9}$$

Thus, the elongation (δ) can be expressed as

$$\delta = \frac{L'-L}{L} = \frac{(7-4n) + 3(2n-3)\cos\theta_c + 6X(n-1)\sin\theta_c}{4n+1} \tag{10}$$

Since

$$\sin\theta_c = \sqrt{\frac{X^2}{1+X^2}} \tag{11}$$

Inserting Eq (11) into Eq (10) yields

$$\delta = \frac{(7-4n) + 3(2n-3)\sqrt{\frac{1}{1+X^2}} + 6(n-1)X\sqrt{\frac{X^2}{1+X^2}}}{4n+1} \tag{12}$$

The maximum elongation can be expressed as

$$\delta_{max} = \lim_{n\to\infty}\delta = 1.5(\sqrt{1+X^2}) - 1 \tag{13}$$

The variation of elongation (δ) with X and n is depicted in Figure S2 of the Supporting Information. Based on this figure and Eqs. (12) and (13), we note that the increase of elongation is insignificant when n>8. When X is fixed, the elongation tends to converge to a constant value as n approaches infinity. Importantly, increasing n is not an efficient way for improving elongation, because the elongation of the ribbon kirigami structure is determined by the ratio of geometric parameters, rather than individual values.

2.4. Computational analysis

The computational analysis of the deformation process of the ribbon kirigami metastructure was performed using Abaqus and Python. The tensile stretching direction was defined as the *y*-axis; the direction orthogonal to the *y*-axis in the stretching plane was taken as the *x*-axis; and the direction perpendicular to the stretching plane was considered the *z*-axis. One end of the model was fully constrained, whereas the other end was allowed to move in the *y*-direction. Two static analysis steps were set to load the model to prevent it from only deforming in the *xy*-plane and from bifurcating due to local buckling of the strips. First, equal and opposite initial displacement disturbances were applied at both ends of the hubs that were along the symmetry axis. The displacement disturbance was along the *z*-axis and was approximately 0.1*c*. Then, the disturbances were removed, and the displacement loading along the *y*-direction was performed. The fixed end was restrained to simulate the boundary condition of the experiments. To ensure convergence, the geometric nonlinearity switch, Nlgeom, was activated. In all simulations, the models were discretized with 3D shell elements (S4R), where all element sizes were 1 mm. Furthermore, for all the models, Abaqus/standard was utilized to simulate the deformation process.

In order to investigate the effect of material, various materials were used for the FEA model, while retaining the same geometric parameters. The material behavior of the ribbon kirigami was captured using an elastoplastic model (material models *ELASTIC and *PLASTIC in Abaqus). The material parameters for the various elastoplastic materials are summarized in Table 1. Moreover, given the findings reported in [67,99], we utilized polyester with an elastic model to investigate how plasticity influenced the deformation process of the ribbon kirigami metastructures.

2.5. Experimental verification

From the previous sections, it was found that the deformation response of the ribbon kirigami structure is primarily dominated by geometric parameters in the first four stages, while the properties of constituent materials began to manifest their influence after the DMT threshold.

Experimental models were fabricated from sheet metals by laser-cutting (Fig. 5A(a-b)). Tensile experiments (Fig. 5A(b-c)) were conducted to verify the accuracy of the prediction model and the results of finite element analyses. Three groups of experiments were designed and conducted, the results of which are summarized in Table 2. The experimental models were made of brass, stainless steel, and Al-3003, and experiments were conducted on a universal tester (Zwick/Roell Z250), as shown in Fig. 5B.

It is important to note that the deformation of the end parts and the elastic strain of the entire structure were neglected in the development of the prediction model. Consequently, the prediction values are slightly lower than the experimental and FEA results, as can be seen from the values in Table 2. It is also worth noting that the ultimate strain of stainless steel 304 is very small (around 0.002), which makes the fifth stage of the deformation process negligible, as shown in Fig. 3. Consequently, the elongation at the onset of fracture of the structure can be approximated by the value at the DMT threshold, which led to a negligible error between the experimental and predicted values. On the other hand, the ultimate strains of brass and Al-3003 are non-negligible, the elastic strains of which result in relatively higher error values. Overall, the prediction model offers a reasonably accurate and flexible method

Table 1
Mechanical properties of different elastoplastic materials.

Material	Density (g/cm^3)	Tensile strength (MPa)	Modulus of elasticity (GPa)	Poisson's ratio	Yield strength (MPa)	Ultimate strain
Steel (Q235)	7.85	400	210	0.30	235	0.200
Al-3003	2.70	324	70	0.33	276	0.200
Brass	8.33	454	109	0.30	104	0.359
Mild steel	7.85	400	200	0.26	200	0.200
Stainless steel	7.85	670	193	0.30	300	0.002

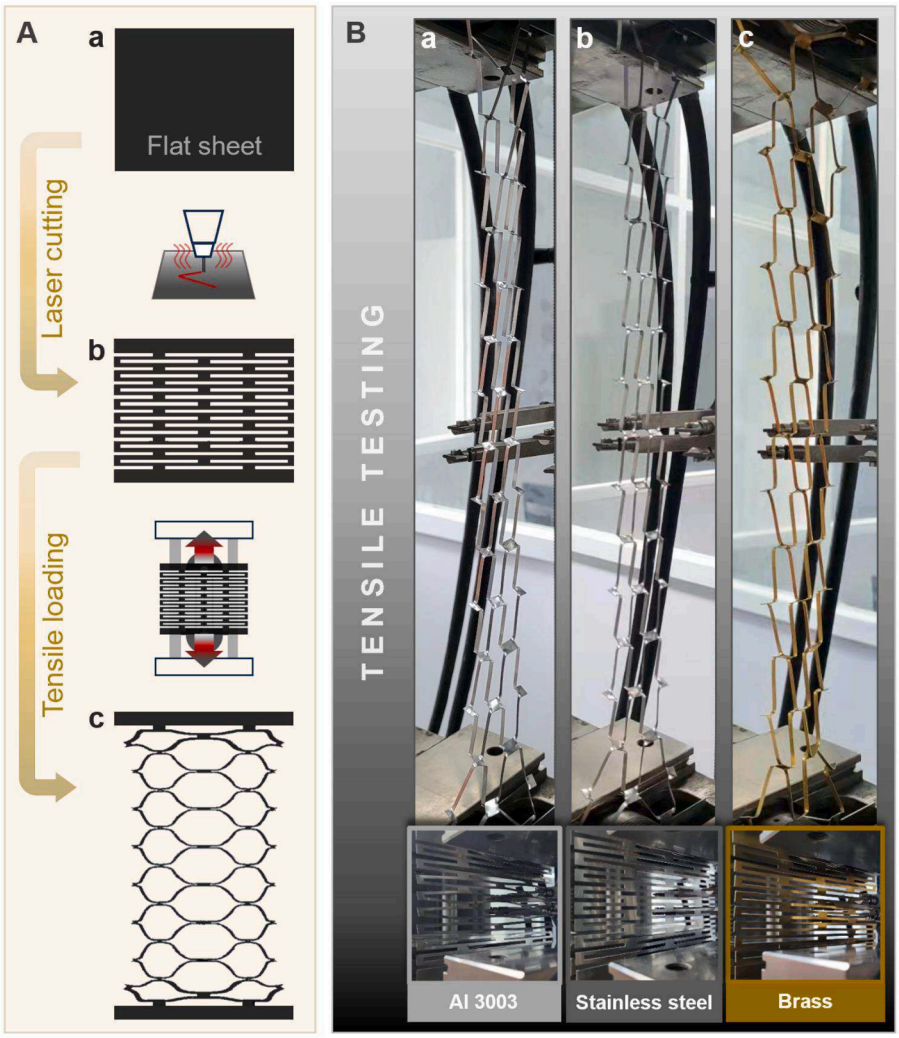

Fig. 5. (**A**) Schematic representations of the (**a**-**b**) fabrication and (**b**-**c**) testing processes of a typical ribbon kirigami specimen. (**B**) Tensile testing of ribbon kirigami specimens made of (**a**) Al-3003, (**b**) stainless steel, and (**c**) brass.

Table 2
Experimental results of tensile testing and their comparison with the corresponding results from the FEA and prediction models.

Material	Experiment	FEA	Prediction	Error (FEA)	Error (prediction)
Al-3003	550.31 %	544.23 %	522.06 %	1.11 %	5.13 %
Brass	554.85 %	535.16 %	522.06 %	3.55 %	5.91 %
Stainless steel	536.36 %	531.16 %	522.06 %	0.98 %	2.74 %

for predicting the elongation of the ribbon kirigami structure.

2.6. Geometric design optimization

In the design and fabrication of kirigami structures, it is often desired to use a minimal amount of material while achieving maximum elongation. Therefore, it is important to optimize the geometric design parameters of such structures. Based on the parameters of Fig. 2a, we can describe the amount of material S as follows

$$S = 8acn + 16bcn + 4bc \tag{14}$$

Here we consider two different optimization scenarios that could have practical implications for the design and manufacturing of such morphing structures. The first scenario is to maximize elongation while

keeping the material volume fixed, which can be expressed as

$$\underset{a,b,c\in\mathbb{R},\ n\in\mathbb{Z}}{\text{Min}} -\frac{7-4n+3(2n-3)\sqrt{\frac{1}{1+X^2}}+6(n-1)X\sqrt{\frac{X^2}{1+X^2}}}{4n+1},\quad \text{where } X=\frac{a-b}{3c}$$

$$\text{s.t. } 8acn+16bcn+4bc-S=0,\ a,b,c,n>0 \tag{15}$$

The second optimization scenario is to minimize the material volume while maintaining a fixed elongation; this problem can be formulated as

$$\begin{aligned}\text{s.t. } &\frac{7-4n+3(2n-3)\sqrt{\frac{1}{1+X^2}}+6(n-1)X\sqrt{\frac{X^2}{1+X^2}}}{4n+1}-\delta=0,\\ &\text{where } X=\frac{a-b}{3c},\ a,b,c,n>0\end{aligned} \tag{16}$$

$$\underset{a,b,c\in\mathbb{R},\ n\in\mathbb{Z}}{\text{Min}}\ 8acn+16bcn+4bc$$

In practice, the range and accuracy of manufacturing and machining processes are limited. As a result, it is necessary to introduce lower bounds and upper bounds for the unknowns *a, b, c,* and *n*, as follows

$$lb_1\leqslant a,b,c\leqslant ub_1 \quad \text{and} \quad lb_2\leqslant n\leqslant ub_2 \tag{17}$$

where lb_1 and lb_2 are the lower bounds, and ub_1 and ub_2 are the upper bounds.

The optimization problems (16) and (17) are Mixed-integer Nonlinear Programming (MINLP) problems. From the formulations above, one can observe that the derivatives with respect to *a, b,* and *c* are so complicated that calculating them may have a heavy computational cost. Moreover, *n* is a positive integer the derivative of which does not exist. Consequently, derivative-based optimization algorithms cannot be used to solve this problem. Furthermore, considering the complexity of expression δ, heuristic algorithms are prone to converging to local rather than global optima. To address these issues, we propose an algorithm employing an exhaustive approach that integrates both genetic algorithms and interior point methods, demonstrating considerable adaptability in parameter optimization for ribbon kirigami structures. Further details of this algorithm are elaborated in Section S1 of the Supporting Information.

As an example, here we consider the optimization problem (16) to demonstrate the performance of the proposed optimization algorithm. Given $\delta = 30,\ 0.01 < a,b,c < 100,$ and $1 < n < 100$, the global minimum of *S*, denoted by S^*, can be found using the abovementioned method as follows

$$\begin{aligned}&a^* = 1.365,\ b^* = 0.01,\\ &c^* = 0.01,\ n^* = 2,\\ &\text{and } S^* = 0.222\end{aligned} \tag{18}$$

where the parameters with the symbol '*' designate the optimal values of the corresponding parameters. The presented algorithm was compared with the standard genetic algorithm as described in Section S2 of the Supporting Information, demonstrating its higher level of accuracy and efficiency in optimizing the parameters of ribbon kirigami metastructures. Moreover, the optimization algorithm can provide optimal values of the geometric parameters of the ribbon kirigami structure with various numbers of units, as summarized in Table 3.

The proposed algorithm provides an efficient approach to optimizing the geometric parameters of the ribbon kirigami structure to meet different requirements.

3. Conclusions

This work investigated the deformation mechanism of a typical ribbon kirigami metastructure by using numerical and experimental methods. We showed that following an initial phase dominated by the geometric design specifications of the ribbon kirigami pattern, there existed a turning point, called the design–material transition (DMT) threshold, after which the deformation behavior was dominated by the properties of the constituent material. Importantly, from an engineering design point of view, the DMT threshold determines a key limit in the deformation capacity of such metastructures for practical applications. Drawing upon this deformation model, an elongation prediction model was established, followed by experimental investigations to validate the accuracy of the model.

Table 3
Optimal geometric parameters for *n*=5 to 10.

n	…	5	6	7	8	9	10	…
a	…	0.8133	0.7765	0.7520	0.7345	0.7213	0.7111	…
b	…	0.0100	0.0100	0.0100	0.0100	0.0100	0.0100	…
c	…	0.0100	0.0100	0.0100	0.0100	0.0100	0.0100	…

The findings of this study demonstrated that the enhancement of elongation through increasing the number of units is limited. In addition, numerical optimization methods were introduced to develop a geometric parameter optimization algorithm in conjunction with the actual manufacturing requirements. Using the proposed optimization framework, designers can obtain the optimal geometric parameters given a set of constraints and requirements.

This work provided insights into the structural mechanics of ribbon kirigami metastructures. Future work in this area could consider more complex geometric patterns with potentially enhanced mechanical properties such as a higher level of ductility. It is anticipated that the results of this study open a path to engineering functional kirigami patterns for the design and fabrication of highly ductile shape-shifting structures.

CRediT authorship contribution statement

Yao Chen: Writing – review & editing, Writing – original draft, Validation, Supervision, Project administration, Methodology, Investigation, Funding acquisition, Formal analysis, Conceptualization. **Ruoqi He:** Writing – review & editing, Writing – original draft, Visualization, Validation, Software, Methodology, Investigation, Formal analysis, Data curation, Conceptualization. **Shun Hu:** Writing – original draft, Software, Investigation, Formal analysis, Data curation. **Ziyang Zeng:** Writing – original draft, Software, Investigation, Formal analysis, Data curation. **Tong Guo:** Writing – original draft, Investigation, Formal analysis, Data curation. **Jian Feng:** Writing – review & editing, Validation, Supervision. **Pooya Sareh:** Writing – review & editing, Visualization, Validation, Supervision, Methodology, Investigation, Formal analysis.

Declaration of competing interest

The authors declare that they have no known competing financial interests or personal relationships that could have appeared to influence the work reported in this paper.

Data availability

Data will be made available on request.

Acknowledgements

This work has been supported by the Natural Science Foundation of Jiangsu Province for Distinguished Young Scientists (Grant No. BK20231517), Southeast University 'Zhongying Young Scholars' project, the Fundamental Research Funds for the Central Universities, and the UK's Engineering and Physical Sciences Research Council (EPSRC Award No. EP/X019470/1).

Appendix A. Supplementary information

Supplementary information to this article can be found online at https://doi.org/10.1016/j.matdes.2024.112979.

References

[1] S. Pellegrino, Deployable structures in engineering, Deployable Structures, Springer, in, 2001, pp. 1–35.
[2] C.P. Klingenberg, M. Barluenga, A. Meyer, Shape analysis of symmetric structures: quantifying variation among individuals and asymmetry, Evolution 56 (2002) 1909–1920.
[3] M.K. Blees, A.W. Barnard, P.A. Rose, S.P. Roberts, K.L. McGill, P.Y. Huang, A.R. Ruyack, J.W. Kevek, B. Kobrin, D.A. Muller, P.L. McEuen, Graphene kirigami, Nature 524 (2015) 204-+. https://doi.org/10.1038/nature14588.
[4] S. Felton, M. Tolley, E. Demaine, D. Rus, R. Wood, A method for building self-folding machines, Science 345 (2014) 644–646, https://doi.org/10.1126/science.1252610.
[5] A. Kuzyk, R. Schreiber, Z. Fan, G. Pardatscher, E.-M. Roller, A. Hoegele, F. C. Simmel, A.O. Govorov, T. Liedl, DNA-based self-assembly of chiral plasmonic nanostructures with tailored optical response, Nature 483 (2012) 311–314, https://doi.org/10.1038/nature10889.
[6] T.C. Shyu, P.F. Damasceno, P.M. Dodd, A. Lamoureux, L. Xu, M. Shlian, M. Shtein, S.C. Glotzer, N.A. Kotov, A kirigami approach to engineering elasticity in nanocomposites through patterned defects, Nat. Mater. 14 (2015) 785-+, https://doi.org/10.1038/nmat4327.
[7] J.L. Silverberg, A.A. Evans, L. McLeod, R.C. Hayward, T. Hull, C.D. Santangelo, I. Cohen, Using origami design principles to fold reprogrammable mechanical metamaterials, Science 345 (2014) 647–650, https://doi.org/10.1126/science.1252876.
[8] Y. Zhang, F. Zhang, Z. Yan, Q. Ma, X. Li, Y. Huang, J.A. Rogers, Printing, folding and assembly methods for forming 3D mesostructures in advanced materials, Nat. Rev. Mater. 2 (2017), https://doi.org/10.1038/natrevmats.2017.19.
[9] E. Jalali, H. Soltanizadeh, Y. Chen, Y.M. Xie, P. Sareh, Selective hinge removal strategy for architecting hierarchical auxetic metamaterials, Communications Materials 3 (2022), https://doi.org/10.1038/s43246-022-00322-7.
[10] P. Zhang, W. Fan, Y. Chen, J. Feng, P. Sareh, Structural symmetry recognition in planar structures using Convolutional Neural Networks, Eng. Struct. 260 (2022) 114227, https://doi.org/10.1016/j.engstruct.2022.114227.
[11] X. Xu, S. Huang, Y. Wang, Y. Luo, A generalized objective function based on weight coefficient for topology-finding of tensegrity structures, App. Math. Model. 115 (2023) 541–567.
[12] P. Sareh, Y. Chen, Intrinsic non-flat-foldability of two-tile DDC surfaces composed of glide-reflected irregular quadrilaterals, Int. J. Mech. Sci. 185 (2020) 105881.
[13] D. Naritomi, N. Hosoya, G. Ando, S. Maeda, H. Shigemune, Creation of origami-inspired honeycomb structure using self-folding paper, Mater. Des. 223 (2022) 111146.
[14] Y. Chen, S. Hu, P. Sareh, Cyclic Reconfigurability of Deployable Ring Structures With Angulated Beams, J. Mech. Robot. 16 (2024) 071005.
[15] D. Han, S. Pal, Y. Liu, H. Yan, Folding and cutting DNA into reconfigurable topological nanostructures, Nat. Nanotechnol. 5 (2010) 712–717, https://doi.org/10.1038/nnano.2010.193.
[16] S. Bangay, From virtual to physical reality with paper folding, Computational Geometry-Theory and Applications 15 (2000) 161–174, https://doi.org/10.1016/s0925-7721(99)00048-6.
[17] Y. Li, J. Yu, K.-H. Ma, J. Shi, 3D paper-cut modeling and animation, Comput. Anim. Virtual Worlds 18 (2007) 395–403, https://doi.org/10.1002/cav.188.
[18] A. Mishra, A. Behera, A critical review on 4D printing and their processing parameters, Int. J. Interact. Des. Manuf. IJIDeM (2023) 1–31.
[19] C. Lor, R. Phon, M. Lee, S. Lim, Multi-functional thermal-mechanical anisotropic metasurface with shape memory alloy actuators, Mater. Des. 216 (2022) 110569, https://doi.org/10.1016/j.matdes.2022.110569.
[20] L. Chang, X. Li, Z. Guo, Y. Cao, Y. Lu, R. Garziera, H. Jiang, On-demand tunable metamaterials design for noise attenuation with machine learning, Mater. Des. 238 (2024) 112685, https://doi.org/10.1016/j.matdes.2024.112685.
[21] B. Wang, J. Zhu, S. Zhong, W. Liang, C. Guan, Space deployable mechanics: A review of structures and smart driving, Mater. Des. 237 (2024) 112557, https://doi.org/10.1016/j.matdes.2023.112557.
[22] Y. Chen, J. Shi, C. Lu, J. Feng, P. Sareh, Hierarchical Clustering-Based Collapse Mode Identification and Design Optimization of Energy-Dissipation Braces Inspired by the Triangular Resch Pattern, J. Struct. Eng. 150 (2024) 04024037.
[23] V. Thakur, R. Singh, R. Kumar, A. Gehlot, 4D printing of thermoresponsive materials: A state-of-the-art review and prospective applications, International Journal on Interactive Design and Manufacturing (IJIDeM) 17 (2023) 2075–2094.
[24] Y. Ke, L.L. Ong, W.M. Shih, P. Yin, Three-Dimensional Structures Self-Assembled from DNA Bricks, Science 338 (2012) 1177–1183, https://doi.org/10.1126/science.1227268.
[25] S. Xu, Z. Yan, K.-I. Jang, W. Huang, H. Fu, J. Kim, Z. Wei, M. Flavin, J. McCracken, R. Wang, A. Badea, Y. Liu, D. Xiao, G. Zhou, J. Lee, H.U. Chung, H. Cheng, W. Ren, A. Banks, X. Li, U. Paik, R.G. Nuzzo, Y. Huang, Y. Zhang, J.A. Rogers, Assembly of micro/nanomaterials into complex, three-dimensional architectures by compressive buckling, Science 347 (2015) 154–159, https://doi.org/10.1126/science.1260960.
[26] Y. Chen, Z. Shao, J. Wei, J. Feng, P. Sareh, Geometric design and performance analysis of a foldcore sandwich acoustic metastructure for tunable low-frequency sound absorption, Finite Elem. Anal. Des. 235 (2024) 104150.
[27] B. Seyidoğlu, A. Rafsanjani, A textile origami snake robot for rectilinear locomotion, Device 2 (2024).
[28] J. Rogers, Y. Huang, O.G. Schmidt, D.H. Gracias, Origami mems and nems, MRS Bull. 41 (2016) 123–129.
[29] D. Dureisseix, An overview of mechanisms and patterns with origami, Int. J. Space Struct. 27 (2012) 1–14.
[30] R.J. Lang, Twists, tilings, and tessellations: Mathematical methods for geometric origami, AK Peters/CRC Press, 2017.
[31] Y. Chen, P. Shi, Y. Bai, J. Li, J. Feng, P. Sareh, Engineered origami crease perforations for optimal mechanical performance and fatigue life, Thin-Walled Struct. 185 (2023) 110572.
[32] Y. Chen, P. Shi, Y. Bai, J. Li, J. Feng, P. Sareh, Effects of perforated creases on the mechanical behavior and fatigue life of thick origami structures, Mech. Based Des. Struct. Mach. (2023) 1–14.
[33] P. Sareh, Symmetric descendents of the Miura-ori, PhD dissertation, Engineering Department, University of Cambridge, 2014.
[34] S. Walker, Form beyond function: practice-based research in objects, environment and meaning, Int. J. Sust. Design 1 (4) (2011) 335–347.
[35] H. Greenough, Form and function: remarks on art, design, and architecture, Univ of California Press, 1969.
[36] P. Sareh, The aesthetics of sustainable industrial design: Form and function in the circular design process, Sustain. Dev. 32 (1) (2024) 1310–1320.
[37] P. Sareh, G. Loudon, The form-affordance-function (FAF) triangle of design, Int. J. Interact. Des. m. (IJIDeM) (2024) 1–21.
[38] F. Leonhardt, The significance of aesthetics in structures, Struct. eng. int. 6 (2) (1996) 74–76.
[39] S.M. Belcastro, T.C. Hull, Modelling the folding of paper into three dimensions using affine transformations, Linear Algebra Appl. 348 (2002) 273–282, https://doi.org/10.1016/s0024-3795(01)00608-5.
[40] P. Sareh, The least symmetric crystallographic derivative of the developable double corrugation surface: Computational design using underlying conic and cubic curves, Mater. Des. 183 (2019), https://doi.org/10.1016/j.matdes.2019.108128.
[41] Y. Chen, C. Lu, J. Yan, J. Feng, P. Sareh, Intelligent computational design of scalene-faceted flat-foldable tessellations, J. Comput. Des. Eng. 9 (2022) 1765–1774.
[42] Y. Chen, R. Xu, C. Lu, K. Liu, J. Feng, P. Sareh, Multi-stability of hexagonal origami hypar based on group theory and symmetry breaking, Int. J. Mech. Sci. 108196 (2023).
[43] C. Lu, Y. Chen, J. Yan, J. Feng, P. Sareh, Algorithmic spatial form-finding of four-fold origami structures based on mountain-valley assignments, J. Mech. Robot. (2023) 1–25.
[44] Y. Chen, C. Lu, W. Fan, J. Feng, P. Sareh, Data-driven design and morphological analysis of conical six-fold origami structures, Thin-Walled Struct. 185 (2023) 110626.
[45] L. Fan, J. Liang, Y. Chen, P. Shi, X. Feng, J. Feng, P. Sareh, Multi-stability of irregular four-fold origami structures, Int. J. Mech. Sci. 268 (2024) 108993.
[46] C. Lu, Y. Chen, W. Fan, J. Feng, P. Sareh, A symmetric substructuring method for analyzing the natural frequencies of conical origami structures, Theor. Appl. Mech. Lett. 100517 (2024).
[47] Y. Chen, P. Sareh, J. Yan, A.S. Fallah, J. Feng, An Integrated Geometric-Graph-Theoretic Approach to Representing Origami Structures and Their Corresponding Truss Frameworks, J. Mech. Des. 141 (2019), https://doi.org/10.1115/1.4042791.
[48] K. Yamaguchi, H. Yasuda, K. Tsujikawa, T. Kunimine, J. Yang, Graph-theoretic estimation of reconfigurability in origami-based metamaterials, Mater. Des. 213 (2022), https://doi.org/10.1016/j.matdes.2021.110343.
[49] P. Sareh, S.D. Guest, Design of isomorphic symmetric descendants of the Miura-ori, Smart Mater. Struct. 24 (2015) 085001.
[50] P. Sareh, S.D. Guest, Design of non-isomorphic symmetric descendants of the Miura-ori, Smart Materials and Structures 24 (2015) 085002.
[51] L.M. Fonseca, M.A. Savi, On the symmetries of the origami waterbomb pattern: kinematics and mechanical investigations, Meccanica 56 (2021) 2575–2598.
[52] R.J. Lang, A computational algorithm for origami design, In (1996) 98–105.
[53] Y. Chen, J. Yan, J. Feng, P. Sareh, Particle swarm optimization-based metaheuristic design generation of non-trivial flat-foldable origami tessellations with degree-4 vertices, Journal of Mechanical Design 143 (2021).
[54] S.J.P. Callens, A.A. Zadpoor, From flat sheets to curved geometries: Origami and kirigami approaches, Mater. Today 21 (2018) 241–264, https://doi.org/10.1016/j.mattod.2017.10.004.
[55] G.P. Collins, Kirigami and technology cut a fine figure, together, Proceedings of the National Academy of Sciences of the United States of America 113 (2016) 240–241. https://doi.org/10.1073/pnas.1523311113.
[56] B. Jang, S. Won, J. Kim, J. Kim, M. Oh, H.-J. Lee, J.-H. Kim, Auxetic Meta-Display: Stretchable Display without Image Distortion, Adv. Funct. Mater. 32 (2022), https://doi.org/10.1002/adfm.202113299.
[57] M. Ouisse, M. Collet, F. Scarpa, A piezo-shunted kirigami auxetic lattice for adaptive elastic wave filtering, Smart Mater. Struct. 25 (2016), https://doi.org/10.1088/0964-1726/25/11/115016.
[58] L. Xu, T.C. Shyu, N.A. Kotov, Origami and Kirigami Nanocomposites, ACS Nano 11 (2017) 7587–7599, https://doi.org/10.1021/acsnano.7b03287.
[59] Y. Chen, W. Ye, R. Xu, Y. Sun, J. Feng, P. Sareh, A programmable auxetic metamaterial with tunable crystal symmetry, Int. J. Mech. Sci. 249 (2023) 108249.
[60] P.Z. Hanakata, Z. Qi, D.K. Campbell, H.S. Park, Highly stretchable MoS2 kirigami, Nanoscale 8 (2016) 458–463, https://doi.org/10.1039/c5nr06431g.

[61] P. Rajak, B. Wang, K. Nomura, Y. Luo, A. Nakano, R. Kalia, P. Vashishta, Autonomous reinforcement learning agent for stretchable kirigami design of 2D materials, Npj Comput. Mater. 7 (2021), https://doi.org/10.1038/s41524-021-00572-y.
[62] S.H. Chen, K.C. Chan, D.X. Han, L. Zhao, F.F. Wu, Programmable super elastic kirigami metallic glasses, Mater. Des. 169 (2019), https://doi.org/10.1016/j.matdes.2019.107687.
[63] L. Dinh Hai, Y. Xu, M.M. Tentzeris, S. Lim, Transformation from 2D meta-pixel to 3D meta -pixel using auxetic kirigami for programmable multifunctional electromagnetic response, Extreme Mech. Lett. 36 (2020), https://doi.org/10.1016/j.eml.2020.100670.
[64] Y. Tang, G. Lin, S. Yang, Y.K. Yi, R.D. Kamien, J. Yin, Programmable Kiri-Kirigami Metamaterials, Adv. Mater. 29 (2017), https://doi.org/10.1002/adma.201604262.
[65] Y. Sun, W. Ye, Y. Chen, W. Fan, J. Feng, P. Sareh, Geometric design classification of kirigami-inspired metastructures and metamaterials, Structures 33 (2021) 3633–3643, https://doi.org/10.1016/j.istruc.2021.06.072.
[66] Y. Zhang, Z. Yan, K. Nan, D. Xiao, Y. Liu, H. Luan, H. Fu, X. Wang, Q. Yang, J. Wang, W. Ren, H. Si, F. Liu, L. Yang, H. Li, J. Wang, X. Guo, H. Luo, L. Wang, Y. Huang, J.A. Rogers, A mechanically driven form of Kirigami as a route to 3D mesostructures in micro/nanomembranes, PNAS 112 (2015) 11757–11764, https://doi.org/10.1073/pnas.1515602112.
[67] A. Rafsanjani, K. Bertoldi, Buckling-induced kirigami, Phys. Rev. Lett. 118 (2017) 084301.
[68] Y. Cho, J.-H. Shin, A. Costa, T.A. Kim, V. Kunin, J. Li, S.Y. Lee, S. Yang, H.N. Han, I.-S. Choi, D.J. Srolovitz, Engineering the shape and structure of materials by fractal cut, in: Proceedings of the National Academy of Sciences of the United States of America 111, 2014, pp. 17390–17395, https://doi.org/10.1073/pnas.1417276111.
[69] Y. Tang, J. Yin, Design of cut unit geometry in hierarchical kirigami-based auxetic metamaterials for high stretchability and compressibility, Extreme Mech. Lett. 12 (2017) 77–85, https://doi.org/10.1016/j.eml.2016.07.005.
[70] Z. Qi, D.K. Campbell, H.S. Park, Atomistic simulations of tension-induced large deformation and stretchability in graphene kirigami, Phys. Rev. B 90 (2014), https://doi.org/10.1103/PhysRevB.90.245437.
[71] T. Castle, Y. Cho, X. Gong, E. Jung, D.M. Sussman, S. Yang, R.D. Kamien, Making the Cut: Lattice Kirigami Rules, Phys. Rev. Lett. 113 (2014), https://doi.org/10.1103/PhysRevLett.113.245502.
[72] A. Flachi, V. Vitagliano, Symmetry breaking and lattice kirigami: Finite temperature effects, Physical Review D 99 (2019) 125010.
[73] T. Han, F. Scarpa, N.L. Allan, Super stretchable hexagonal boron nitride Kirigami, Thin Solid Films 632 (2017) 35–43.
[74] Z. Liu, H. Du, J. Li, L. Lu, Z.-Y. Li, N.X. Fang, Nano-kirigami with giant optical chirality, Sci. Adv. 4 (2018), https://doi.org/10.1126/sciadv.aat4436.
[75] P. Shi, Y. Chen, J. Feng, P. Sareh, Highly stretchable graphene kirigami with tunable mechanical properties, Phys. Rev. E 109 (2024) 035002.
[76] P. Shi, Y. Chen, Y. Wei, J. Feng, T. Guo, Y. Tu, P. Sareh, Deformation response of highly stretchable and ductile graphene kirigami under uniaxial and biaxial tension, Phys. Rev. B 108 (2023) 134105.
[77] S.H. Chen, H.Y. Cheng, K.C. Chan, G. Wang, Metallic glass structures for mechanical-energy-dissipation purpose: a review, Metals 8 (2018), https://doi.org/10.3390/met8090689.
[78] D. Han, S. Chen, L. Zhao, X. Tong, K. Chan, Architected hierarchical kirigami metallic glass with programmable stretchability, AIP Adv. 12 (2022).
[79] S.H. Chen, K.C. Chan, T.M. Yue, F.F. Wu, Highly stretchable kirigami metallic glass structures with ultra-small strain energy loss, Scr. Mater. 142 (2018) 83–87, https://doi.org/10.1016/j.scriptamat.2017.08.037.
[80] K. Xu, Y. Lu, S. Honda, T. Arie, S. Akita, K. Takei, Highly stable kirigami-structured stretchable strain sensors for perdurable wearable electronics, J. Mater. Chem. C 7 (2019) 9609–9617.
[81] N. Zheng, Z. Fang, W. Zou, Q. Zhao, T. Xie, Thermoset shape-memory polyurethane with intrinsic plasticity enabled by transcarbamoylation, Angewandte Chemie-International Edition 55 (2016) 11421–11425, https://doi.org/10.1002/anie.201602847.
[82] W. Zheng, W. Huang, F. Gao, H. Yang, M. Dai, G. Liu, B. Yang, J. Zhang, Y.Q. Fu, X. Chen, Y. Qiu, D. Jia, Y. Zhou, P. Hu, Kirigami-inspired highly stretchable nanoscale devices using multidimensional deformation of monolayer MoS2, Chem. Mater. 30 (2018) 6063–6070, https://doi.org/10.1021/acs.chemmater.8b02464.
[83] S. Huang, Y. Liu, Y. Zhao, Z. Ren, C.F. Guo, Flexible Electronics: Stretchable Electrodes and Their Future, Adv. Funct. Mater. 29 (2019), https://doi.org/10.1002/adfm.201805924.
[84] Y. Bao, G. Hong, Y. Chen, J. Chen, H. Chen, W.-L. Song, D. Fang, Customized kirigami electrodes for flexible and deformable lithium-ion batteries, ACS Appl. Mater. Interfaces 12 (2020) 780–788, https://doi.org/10.1021/acsami.9b18232.
[85] Z. Song, X. Wang, C. Lv, Y. An, M. Liang, T. Ma, D. He, Y.-J. Zheng, S.-Q. Huang, H. Yu, H. Jiang, Kirigami-based stretchable lithium-ion batteries, Sci. Rep. 5 (2015), https://doi.org/10.1038/srep10988.
[86] M. Yang, H. Wang, W. Shuai, X. Deng, Thermal optimization of a kirigami-patterned wearable lithium-ion battery based on a novel design of composite phase change material, Appl. Therm. Eng. 161 (2019), https://doi.org/10.1016/j.applthermaleng.2019.114141.
[87] B. Gao, A. Elbaz, Z. He, Z. Xie, H. Xu, S. Liu, E. Su, H. Liu, Z. Gu, Bioinspired kirigami fish-based highly stretched wearable biosensor for human biochemical-physiological hybrid monitoring, Advanced Materials Technologies 3 (2018), https://doi.org/10.1002/admt.201700308.
[88] A. Rafsanjani, Y. Zhang, B. Liu, S.M. Rubinstein, K. Bertoldi, Kirigami skins make a simple soft actuator crawl, Sci. Rob. 3 (2018), https://doi.org/10.1126/scirobotics.aar7555.
[89] A. Lamoureux, K. Lee, M. Shlian, S.R. Forrest, M. Shtein, Dynamic kirigami structures for integrated solar tracking, Nat. Commun. 6 (2015), https://doi.org/10.1038/ncomms9092.
[90] Y. Li, K. Chang, J. Chang, B. Yu, L. Liu, B. Liu, X. Zhao, W. Deng, Printed Kirigami Organic Photovoltaics for Efficient Solar Tracking, Adv. Funct. Mater. 32 (2022), https://doi.org/10.1002/adfm.202204004.
[91] Y.J. Ke, Y. Yin, Q.T. Zhang, Y.T. Tan, P. Hu, S.C. Wang, Y.C. Tang, Y. Zhou, X. L. Wen, S.F. Wu, T.J. White, J. Yin, J.Q. Peng, Q.H. Xiong, D.Y. Zhao, Y. Long, Adaptive thermochromic windows from active plasmonic elastomers, Joule 3 (2019) 858–871, https://doi.org/10.1016/j.joule.2018.12.024.
[92] N.-S. Jang, K.-H. Kim, S.-H. Ha, S.-H. Jung, H.M. Lee, J.-M. Kim, Simple approach to high-performance stretchable heaters based on kirigami patterning of conductive paper for wearable thermotherapy applications, ACS Appl. Mater. Interfaces 9 (2017) 19612–19621.
[93] H. Zhou, Y. Zhang, Y. Qiu, H. Wu, W. Qin, Y. Liao, Q. Yu, H. Cheng, Stretchable piezoelectric energy harvesters and self-powered sensors for wearable and implantable devices, Biosens. Bioelectron. 168 (2020), https://doi.org/10.1016/j.bios.2020.112569.
[94] D.X. Han, L. Zhao, S.H. Chen, G. Wang, K.C. Chan, Critical transitions in the shape morphing of kirigami metallic glass, J. Mater. Sci. Technol. 61 (2021) 204–212, https://doi.org/10.1016/j.jmst.2020.05.065.
[95] M. Moshe, E. Esposito, S. Shankar, B. Bircan, I. Cohen, D.R. Nelson, M.J. Bowick, Kirigami Mechanics as Stress Relief by Elastic Charges, Phys. Rev. Lett. 122 (2019), https://doi.org/10.1103/PhysRevLett.122.048001.
[96] K. Chen, M. Yuan, H.M. Zheng, S.H. Chen, On the determination and optimization of apparent “elastic limit” of kirigami metallic glasses, Physica B-Condensed Matter 609 (2021), https://doi.org/10.1016/j.physb.2021.412901.
[97] M. Isobe, K. Okumura, Continuity and discontinuity of kirigami’s high-extensibility transition: A statistical-physics viewpoint, Physical Review Research 1 (2019), https://doi.org/10.1103/PhysRevResearch.1.022001.
[98] M.A. Dias, M.P. McCarron, D. Rayneau-Kirkhope, P.Z. Hanakata, D.K. Campbell, H. S. Park, D.P. Holmes, Kirigami actuators, Soft Matter 13 (2017) 9087–9092, https://doi.org/10.1039/c7sm01693j.
[99] N. An, A.G. Domel, J. Zhou, A. Rafsanjani, K. Bertoldi, Programmable hierarchical kirigami, Adv. Funct. Mater. 30 (2020) 1906711.